Micro-hexapod robot with an origami-like SU-8-coated rigid frame

Kenjiro Sugimoto and Sumito Nagasawa

Mechanical Engineering Graduate School, Shibaura Institute of Technology, Micro robotics laboratory, Tokyo, Japan
Corresponding author: Sumito Nagasawa; Email: nagasawa@shibaura-it.ac.jp

Abstract

In recent years, many microrobots have been developed for search applications using swarms in places where humans cannot enter, such as disaster sites. Hexapod robots are suitable for moving over uneven terrain. In order to use micro-hexapod robots for swarm exploration, it is necessary to reduce the robot's size while maintaining its rigidity. Herein, we propose a micro-hexapod with an SU-8 rigid frame that can be assembled from a single sheet. By applying the SU-8 coating as a structure to the hexapod and increasing the rigidity, the substrate size can be reduced to within $40\,\text{mm} \times 40\,\text{mm}$ and the total length when assembled to approximately $30\,\text{mm}$. This enables the integration of the micro electromechanical systems (MEMS) process into small and inexpensive hexapod robots. In this study, we assembled the hexapod with a rigid frame from a sheet created using the MEMS process and evaluated the leg motion.

1. Introduction

In recent years, many microrobots have been developed for search applications using swarms in places where humans cannot enter, such as disaster sites [1–3]. A hexapod robot is suitable for rugged terrain and is effective for these activities [4–8]. The hexapod robot walks according to the tripod gait. When walking in the tripod gait, a combination of three legs (right front (RF), left middle (LM), and right rear (RR) legs) touches the ground, making a triangle that supports the center of mass. This triangle is known as a supporting polygon. The remaining three legs perform a forward walking motion [9–11]. The following hexapod robots: HAMR [12], RoACH [13], VelociRoACH [14–18], DASH [19], Rhex [20, 21], and iSprawl [22, 23] realize walking motion on rough terrain, such as inclines and declines or obstacles, and are investigated further. Additionally, from the viewpoint of efficiency and cost, for search applications using these hexapod robots, multi-agent searching using a swarm algorithm is compared to searching using a high-performance and expensive sole robot [24, 25].

Microrobots must be produced at a low cost for swarm applications. However, this is a challenging task because the grip, alignment, and assembly of miniaturized parts are required for microrobot assembly. Therefore, robots that are folded and assembled have received much attention because they do not require the grip, alignment, and assembly of parts [26–28]. In a previous study, the fabrication of a hexapod assembled from a single flat Flexible Printed Circuit (FPC) sheet was proposed. Since complicated assembly processes are not required, a hexapod can be assembled at a low cost [29]. In our previous study, the rigid parts of the body frame were realized by folding an FPC sheet and creating a truss structure, as shown in Fig. 1(b). However, the truss structure of the FPC sheet was not used throughout the robot, and the frame was slightly deformed by the frame movement due to insufficient rigidity in the frame of the main body. This frame distortion caused inefficient movement of the drive links.

In this study, a rigid part using SU-8 3050 (negative photoresist, Tokyo Ohka Kogyo Co., Ltd.) and thick photoresist for high-aspect structures is proposed as an alternative to the folding FPC sheet truss
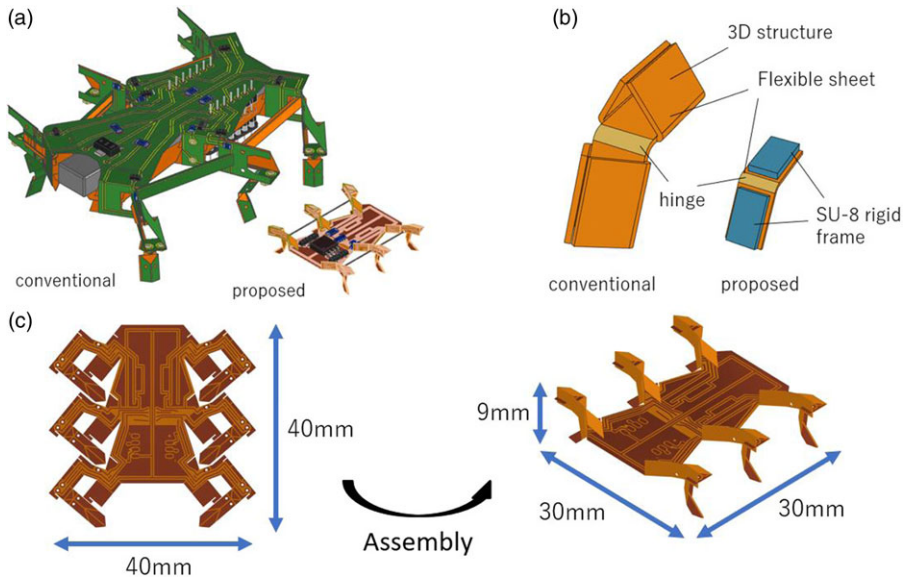
Figure 1. *Miniaturized hexapod using SU-8 board; (a) size comparison between a hexapod of the previous study and hexapod according to proposed method. (b) Miniaturization of the joint structure using the proposed SU-8 board. (c) Size of SU-8 hexapod board and the dimensions of the assembled hexapod.*
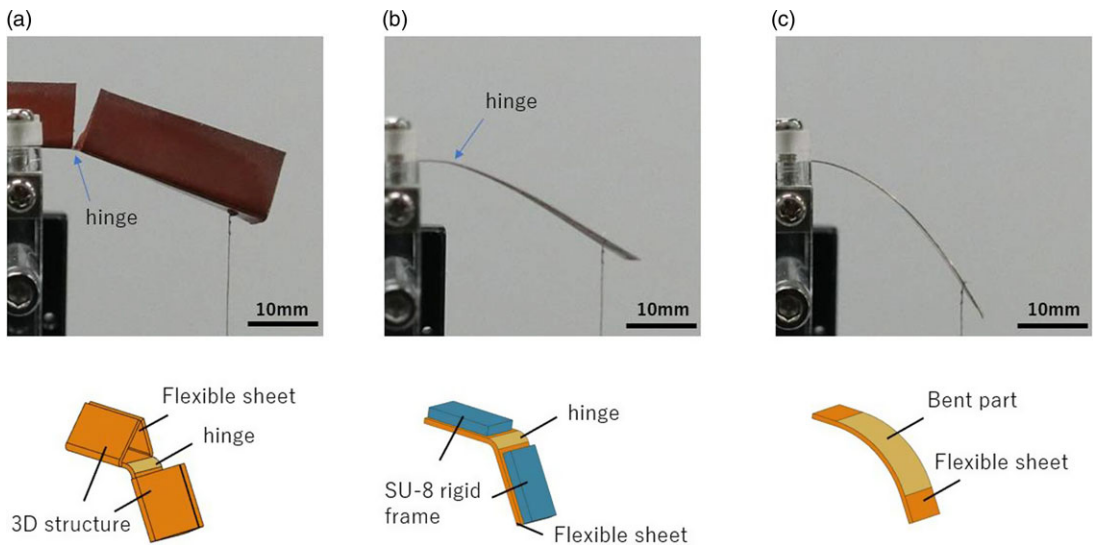

Figure 2. *Comparison of rigidity of hinges by leg structure. A 3 g weight is attached to the tip of each leg structure (10 mm wide) for comparison. (a) Leg structure with conventional truss structure, (b) SU-8 coated leg structure and (c) flexible sheet-only leg structure.*

structure. The SU-8 rigid part has sufficient rigidity to effectively operate the driving linkage. As shown in Fig. 1(a), because the folding process of the rigid part is unnecessary and micro electromechanical systems (MEMS) techniques can be applied to the SU-8 process, further miniaturization of the hexapod is expected.

Fig. 2 demonstrates that both the conventional leg structure and the leg structure coated with SU-8 exhibit equivalent effectiveness as hinges when force is applied. Fig. 2(a) shows that the conventional truss structure of the leg possesses sufficient rigidity to function as a hinge. Figs. 2(b) and 2(c) present a
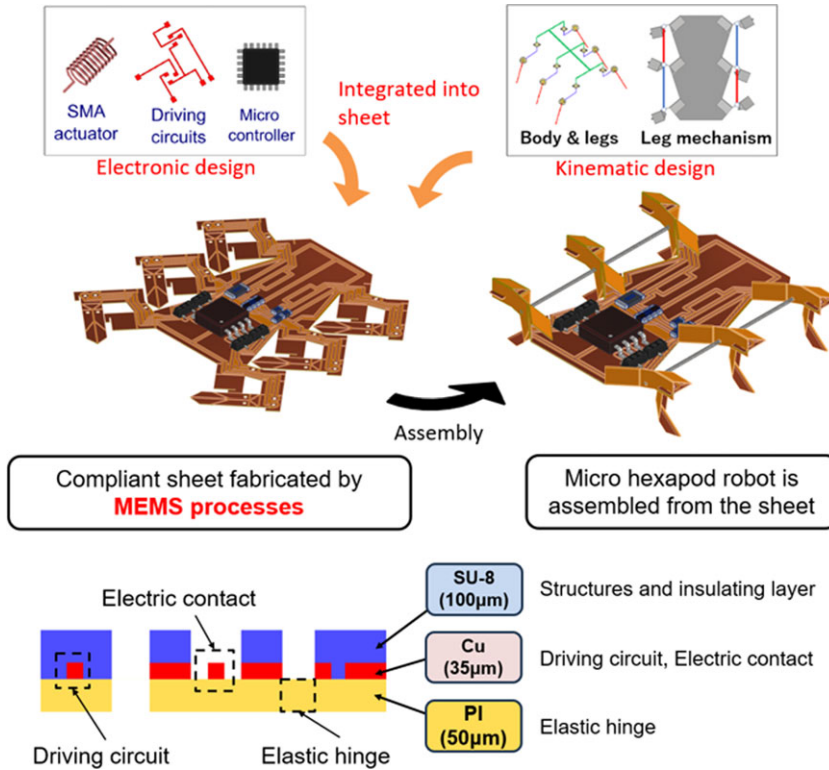
Figure 3. *Micro hexapod robot assembled using a proposed SU-8 board.*

comparison of leg structures with and without SU-8 coating. The displacement at the tensile point was 11.5 mm for the truss structure in (a), 15.5 mm for the structure with SU-8 coating in (b), and 24.4 mm for the structure without coating in (c). The leg structure with SU-8 coating showed almost no deformation at the coated parts, deforming primarily at the hinge section, thereby exhibiting a function similar to a joint in the truss structure. The bending rigidity, EI, derived from curvature and load, was 91.8 [Nmm^2] for (b) and 35.8 [Nmm^2] for (c), indicating that the application of SU-8 coating resulted in approximately 2.5 times greater bending rigidity. The SU-8 coating creates a significant difference in rigidity between the stiff parts and the hinge, allowing the hinge section to function effectively as a joint in a robot.

The hexapod fabricated in this study improved the rigidity of the body frame by coating SU-8 (100 μm thickness) as a structure on an FPC sheet of copper (Cu 35 μm) / polyimide (PI 50 μm). Hereinafter, this is called a "SU-8 board." As shown in Fig. 1(c), applying the MEMS process to the SU-8 board fabrication process downsized the SU-8 board to within a 40 mm square, and the assembled hexapod body length was miniaturized to approximately 30 mm.

The objective of this study is to establish a fabrication method for a micro-hexapod assembled from the proposed SU-8 board, as shown in Fig. 3. Using the MEMS processes, electrical circuits (shape memory alloy (SMA) driving circuit, power supply circuit, microcontroller, etc.) and functional structures (body frame, six legs, driving linkage, etc.) are integrated into the SU-8 board. To confirm the SU-8 rigidity, the movement of the leg fabricated with the proposed SU-8 board was measured.

2. Micro hexapod design using the MEMS process

2.1. Design concept

Fig. 4(a) shows a model of a hexapod fabricated using MEMS processes. The total length of the hexapod is approximately 30 mm, and the hexapod was assembled by simply folding the SU-8 board. The elastic hinges (Cu on the PI layer) of the hexapod are driven by the Ti-Ni SMA actuator. The Ti-Ni SMA
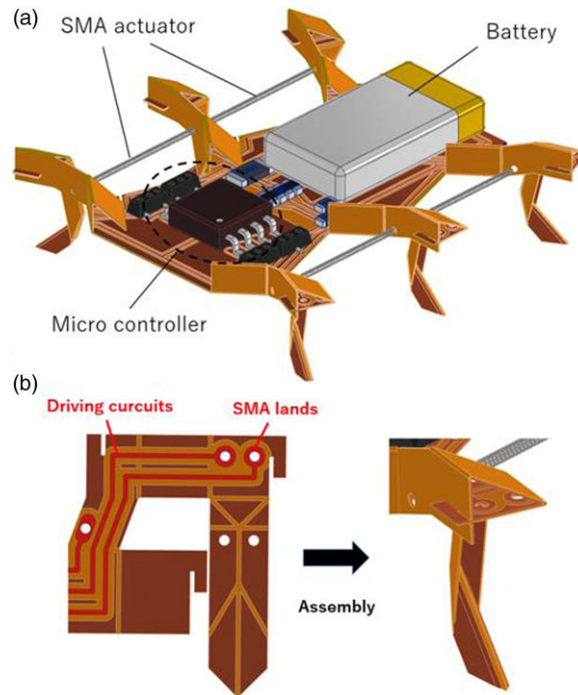
Figure 4. *Proposing method: (a) Hexapod model, (b) leg assembly structure.*

actuator has the same electrical resistance as a nichrome wire and can be operated by Joule heating [30]. This heating method is called energization heating and is generally used for micro robot actuation [31].

At the microscale, because the convective heat radiation from the SMA surface dominates the heat capacity of the SMA volume, the SMA actuator used in microrobots exhibits a good response [32].

The elastic hinge of the hexapod joint consisted of Cu and PI layers. The SMA actuator attached to the elastic hinge shrank when the SMA was energized and Joule heat was generated; subsequently, the elastic hinge was bent. After stopping the heating, the SMA is stretched by restoring the force of the elastic hinge, which functions like a spring.

Fig. 4(b) shows the assembled structure of the legs of the SU-8 board. Since the "inside reverse fold" is employed for the toe structure, the rigidity of the toe is sufficiently increased to support the whole hexapod weight. Electric circuit wires made of Cu were designed along the leg shape, and SMA lands for attaching the SMA actuator were formed at the end of the wire.

Fig. 3 shows a cross-sectional view of the SU-8 board. The SU-8 board consists of three layers: polyimide (PI), copper (Cu), and SU-8. As shown in Fig. 4(b), owing to its flexibility, the PI layer is utilized not only for elastic hinges in robot joints but also for the folding creases of the origami frame. The Cu layer plays two roles: elastic hinges and electric circuit wires. It is difficult to generate the required elastic force using only the PI layer, which restores the force of the elastic hinge and uses it for hexapod walking motion. Therefore, a Cu layer was added to the PI elastic hinge to strengthen the elastic force. The Cu pattern is also used for electrical wiring between the SMA actuators, battery, and microcontroller. Given that the Cu pattern on the elastic hinge can be used as an electric wire, external circuit boards or jumping wires are not required. The SU-8 layer improves the rigidity of the robot frames. Using this SU-8 rigid frame, the three-dimensional folded truss structure required in our previous study can be omitted. By coating the board surface, except for the joints, bends, electrical components, and SMA lands with SU-8, the SU-8 layer also functions as a surface insulation resistance (SIR). The SIR prevents electrical shorting between the SMA and Cu layers. The SU-8 layer creates a significant rigidity difference between the rigid part of the frame and the elastic hinge [33].
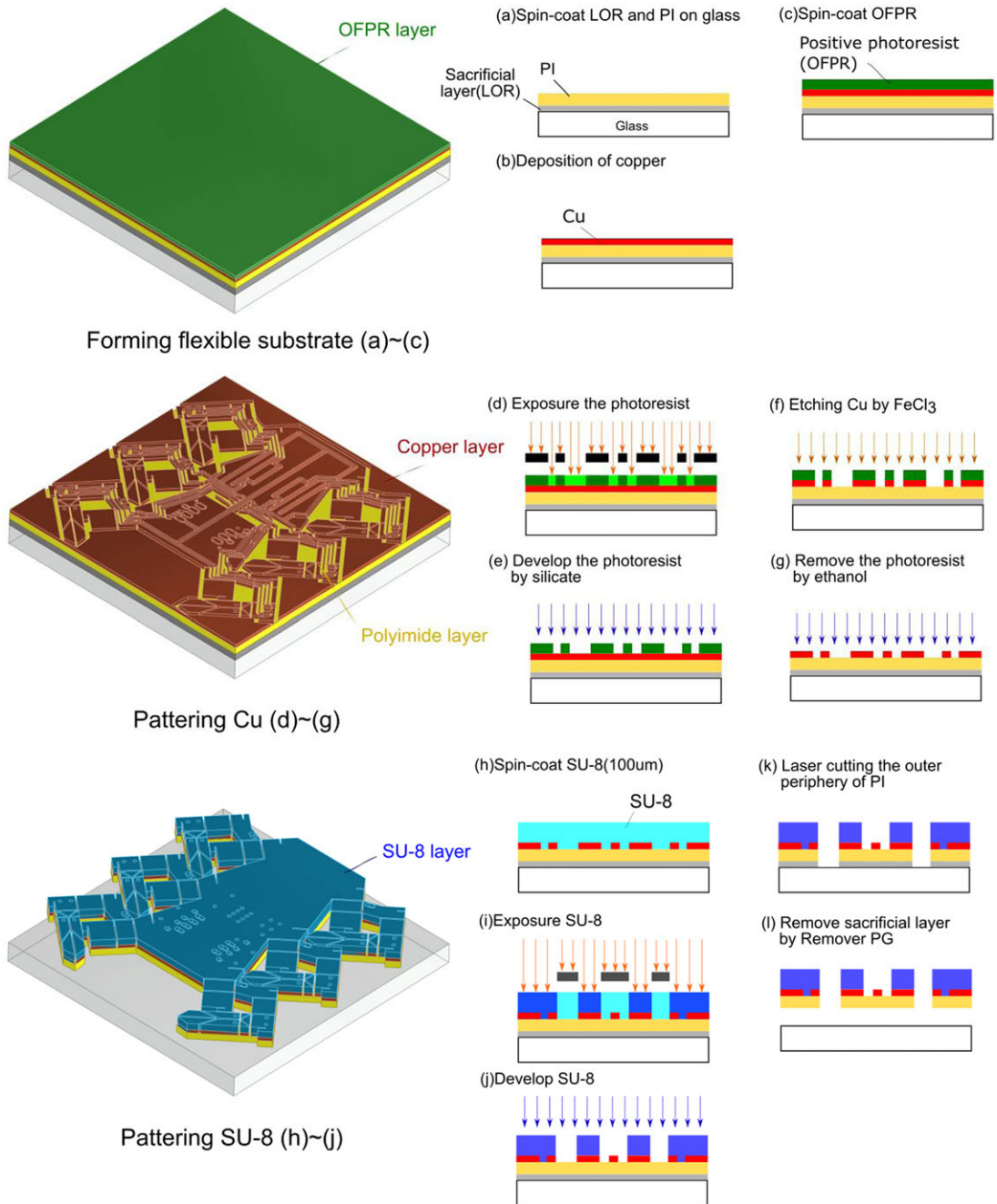
OFPR layer

(a)Spin-coat LOR and PI on glass

Sacrificial layer(LOR)   PI

Glass

(b)Deposition of copper

Cu

(c)Spin-coat OFPR

Positive photoresist (OFPR)

Forming flexible substrate (a)~(c)

Copper layer

(d) Exposure the photoresist

(e) Develop the photoresist by silicate

(f) Etching Cu by FeCl₃

(g) Remove the photoresist by ethanol

Polyimide layer

Pattering Cu (d)~(g)

SU-8 layer

(h)Spin-coat SU-8(100um)

SU-8

(i)Exposure SU-8

(j)Develop SU-8

(k) Laser cutting the outer periphery of PI

(l) Remove sacrificial layer by Remover PG

Pattering SU-8 (h)~(j)

Figure 5. *MEMS fabrication process for SU-8 board.*

2.2. MEMS fabrication process for SU-8 board

Fig. 5 shows the flow of the MEMS process. First, from (a) to (c), a multilayer flexible substrate was formed using material deposition equipment. In process (a), the LOR layer is a sacrificial layer, and the PI layer is used as an elastic hinge. These layers were then spin-coated onto a glass substrate. In process (b), a Cu layer is used as the elastic hinge, and electric circuit wiring is formed by sputtering. Then, OFPR800-20 cp (positive photoresist, Tokyo Ohka Kogyo Co., Ltd.) was spin-coated on the Cu layer in
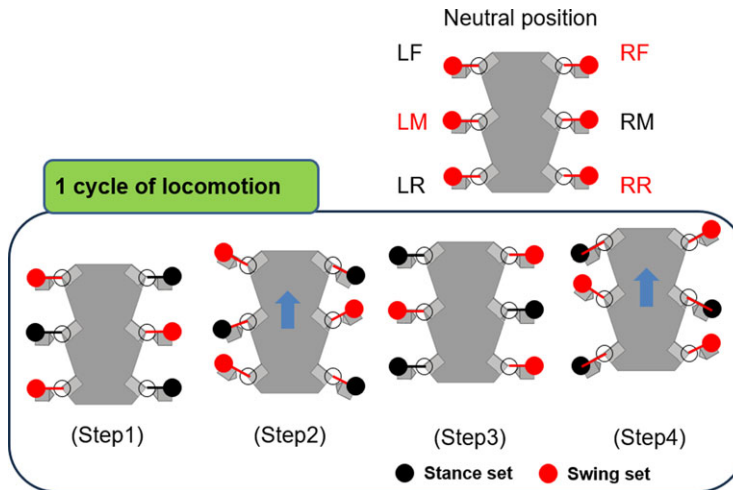
Figure 6. *Single cycle of walking locomotion by tripod gate.*

process (c). In this study, a flexible board (NZ-M3K) manufactured by Sunhayato Corp., which had the same structure as the result of processes (a) through (c), was used. In processes (d)–(g), the Cu layer was patterned. In processes (d) and (e), OFPR800 was exposed to ultraviolet (UV) light and developed with a photoresist developer (DP-1000, Sunhayato Corp.). In process (f), the Cu layer was etched using ferric chloride (FeCl3). Finally, OFPR800 was removed using ethanol in process (g).

In processes (h) to (l), an SU-8 layer ($100\,\mu$m) was spin-coated on the Cu and PI layers as a hexapod structure and patterned. MicroChem SU-8 3000 was used for this process. In process (i), SU-8 is UV-cured, which is required structurally. Unnecessary SU-8 is developed and removed in process (j). In process (k), the PI and LOR (sacrificial layer, Tokyo Ohka Kogyo Co., Ltd.) layers are cut into hexapod molds with a laser cutter. Finally, in process (l), the sacrificial layer is removed with Remover PG (exfoliation solution, Tokyo Ohka Kogyo Co., Ltd.), and the completed sheet is removed from the glass substrate. (When using NZ-M3K, acetone was used to remove the sacrificial layer.)

The completed SU-8 board (Fig. 6) was a hexapod mold consisting of a PI layer as the elastic hinge, a Cu layer as the wiring shape, and SU-8 as the structure. It can be electrically equipped and assembled into a hexapod.

2.3. Operation mode

BMX100 (Bio-metal helix, $100\,\mu$m coil wire diameter) manufactured by Toki Corporation was selected as the SMA actuator for leg movement. This actuator is a coiled Ti–Ni functional anisotropic shape memory alloy (FASMA), which is small and deformation-prone with a high contraction force. The BMX100 has a coil diameter of 0.4 mm, a deformation range of approximately 50% of its natural length, and a contraction force of 0.1–0.2 N. The required specifications for the operation of our hexapod were to walk straight ahead and then turn. The legs of the robot have three segments: the coxa, femur, and tibia. The legs consist of a Coxa-Femur (C-F) joint that operates horizontally with respect to the ground and a Femur-Tibia (F-T) joint that operates vertically. Our hexapod has two modes of operation (Fig. 7). The horizontal operation mode is called Mode 1, and the vertical operational mode is called Mode 2. Walking was achieved by combining the two operation modes.

Fig. 6 shows one cycle of the walking motion. A tripod gait, a common hexapod gait, was used for walking. The RF, LM leg, and RR leg are the first leg groups, and the left foreleg (LF), right middle leg (RM), and left rear leg (LR) are the second leg groups. Each leg group is operated simultaneously during walking. While the first leg group is in the standing leg set and supporting the body in the natural
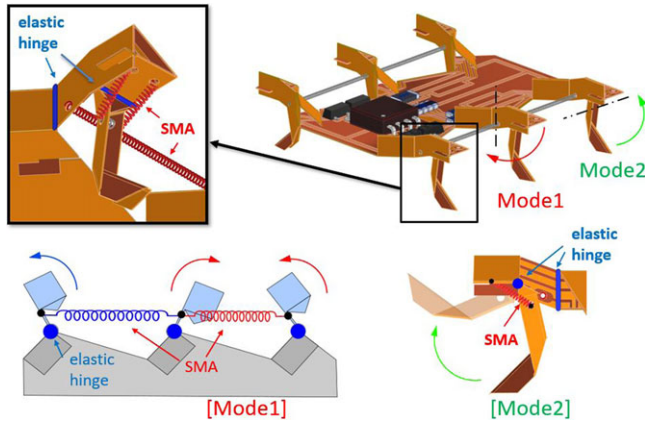
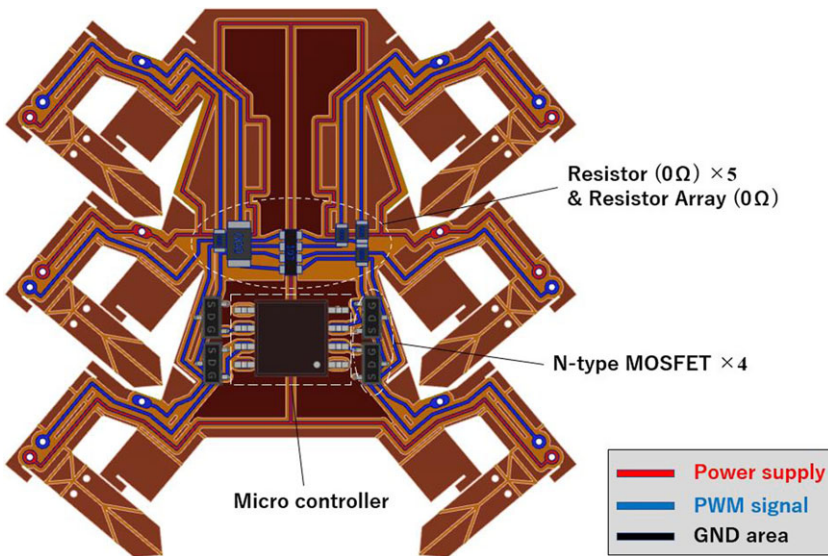**Figure 7.** *Operation mode of the hexapod robot.*

Figure 8. *Hexapod circuit design and electrical component layout.*

posture, the other second leg group is in the swinging leg set with the leg raised in Mode 2 operation (Step 1). While the stance leg set is supporting the body, the swinging leg set is moved forward and the stance leg set is moved backward in a Mode 2 motion to perform a forward movement (Step 2), and then the stance leg set and swinging leg set are swapped in a Mode 2 motion (Step 3). In the same way, the walking motion is performed by moving the stance leg set backward and the swinging leg set forward in a Mode 2 motion (Step 4). By repeating this cycle, a tripod gait, which is a walking motion, is realized.

2.4. Circuit design

Fig. 8 shows the circuit pattern of the SU-8 board, and Fig. 9 shows the circuit control block diagram. In this drive circuit, to realize a tripod gait with fewer controls, in Mode 2 operation, there are the first leg groups, namely, RF, LM, and RR, and the second leg groups, namely, LF, RM, and LR. Moreover, the switching circuit in each group was connected to a $0\,\Omega$ resistor so that the three legs could be driven simultaneously. In the Mode 1 drive circuit, only two SMAs are used on the left and right sides, and
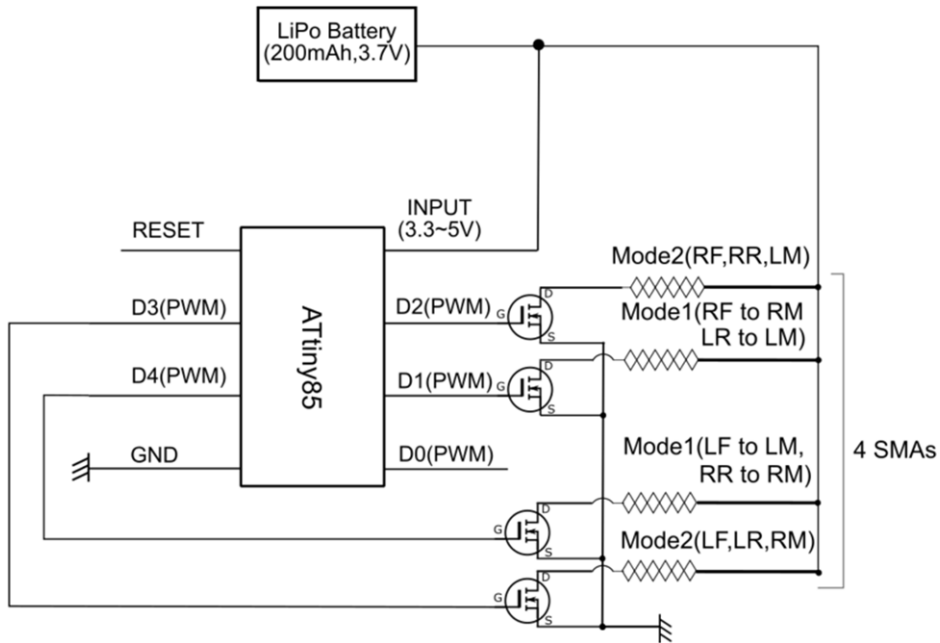
Figure 9. *Hexapod circuit control block diagram.*

the circuit is soldered at three points: the forefoot, middle leg, and hindfoot through the middle leg. At the time of driving, it is controlled by a circuit that switches between the forefoot and hindfoot. In this drive circuit, six SMAs are controlled by a total of four pulse width modulation (PWM) outputs: 2 for Modes 1 and 2 for Mode 2. Therefore, the ATtiny85 was selected as the microcontroller, which is capable of four PWM outputs. A lithium polymer battery (200 mAh, 3.7 V) was used as the drive power supply, and the PWM signals were switched using an N-channel MOSFET (HEXFET – IRF L8244 TRPbF manufactured by Infineon Technologies). A PWM signal was input from the ATtiny85 to each N-channel MOSFET, the heating ratio of the SMA was controlled, and the robot operated. The microcontroller, N-channel MOSFET, and $0\,\Omega$ resistor were mounted on the pad of the hexapod board, and the SMA was mounted on the land by soldering.

3. Experimental results and methods

3.1. Fabrication and assembly of SU-8 board

Figure 10(a) shows an SU-8 board fabricated using the MEMS process. Fig. 10(b) shows the tip of the leg and the wiring part, and Fig. 11(c) shows an enlarged tip of the foot. The composition of each layer consists of a PI, Cu, and SU-8 layer from the bottom. Fig. 10(b) shows the composition and thickness of each layer. The PI layer is brown at the bottom, followed by the Cu layer, which is copper-colored with a metallic luster, and finally the transparent SU-8 layer at the top.

Fig. 11 shows a hexapod substrate produced by the MEMS process and a hexapod robot assembled from the SU-8 board. The total length of the main body of the hexapod robot was 30 mm, and the weight of the body frame was 0.4 g. The weight of each component is listed in Table I, and the combined weight was 2.17 g.

3.2. Driving experiment in operation mode

A drive experiment was performed in the operation mode of the hexapod. Fig. 12 shows the experimental setup of the driving experiment. In this experiment, the SMA actuator is used to drive Mode 1, horizontal

Table I. *Weight of each component of the hexapod.*

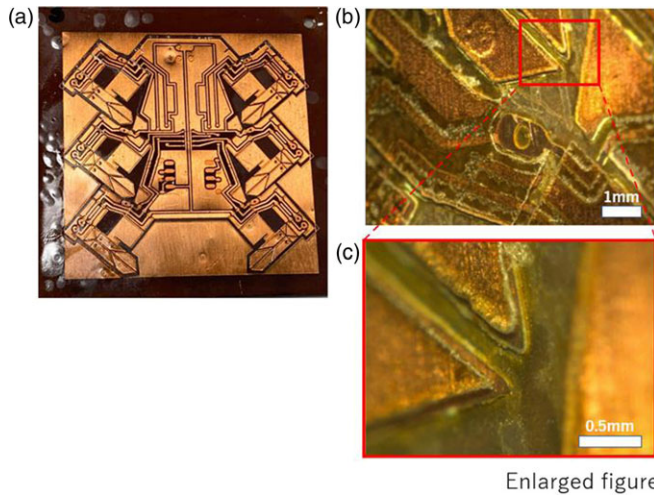| Component	Mass (mg)
SU-8	400
Electronic components	160
Battery	1600
Actuators	10
Total mass	2170

Figure 10. *MEMS process. (a) SU-8 board. (b)(b) Leg tips and wiring area. (c) Enlarged view of leg tips.*
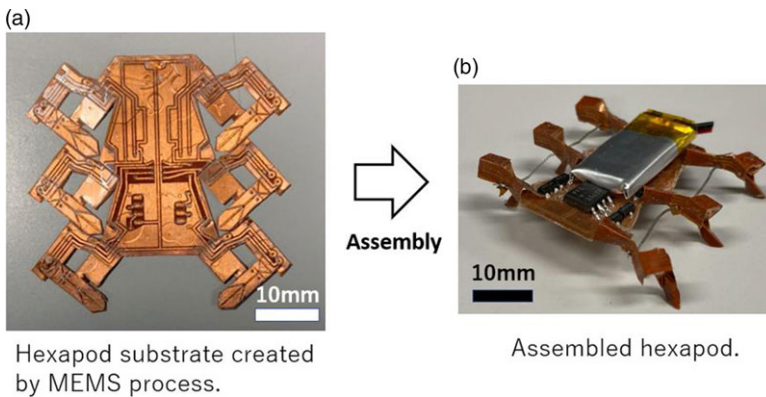

Figure 11. *SU-8 board assembly. (a) SU-8 board (b) Assembled hexapod.*

leg movement, and Mode 2, vertical leg movement. The purpose of this experiment was to investigate the driveable range and responsiveness of toes and to confirm whether they have sufficient obstacle traversability. Markers were attached to the tips and bases of the legs, motion images were taken using a camera, and the trajectory of the marker on the toes was measured by image analysis using ImageJ software. Simultaneously, we conducted experiments on the effective voltage and operating angle by using PWM control.
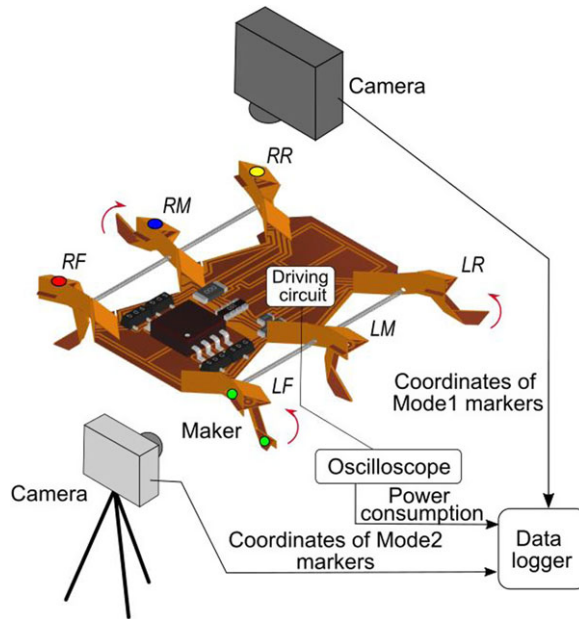
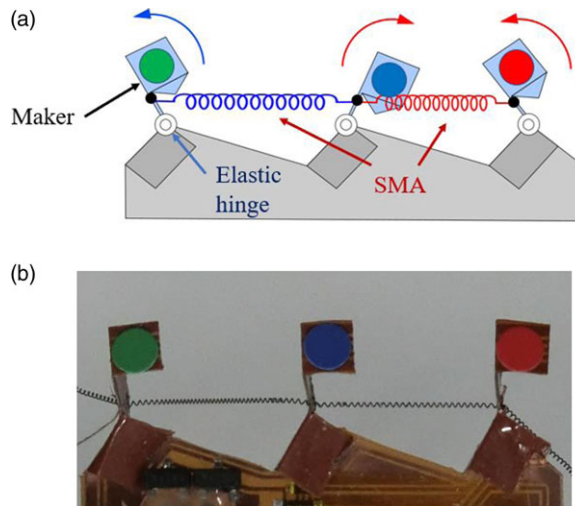**Figure 12.** *Experimental setup for operation testing.*

Figure 13. *Experimental setup for Mode 1 testing: (a) Schematic diagram of Mode 1. (b) Photo image of Mode 1.*

3.2.1. Driving experiment for operating Mode 1

We conducted a motion experiment on Mode 1, a horizontal leg movement using an SMA. As shown in Fig. 12, in the Mode 1 drive circuit, a single SMA is connected to the circuit at three points (front leg, middle leg, and rear leg), and the switching circuit of the front or rear leg controls the drive. In the experiment, the circuit for switching was used to contract the SMA between the foreleg and the middle leg, and between the middle and hind legs by energized heating, alternating between the two legs. Fig. 13(a) shows a schematic diagram of the operation of the SMA between the middle and hind legs. The foreleg without SMA operation is restored to its initial position by the restoring force of the elastic hinge at the joint.
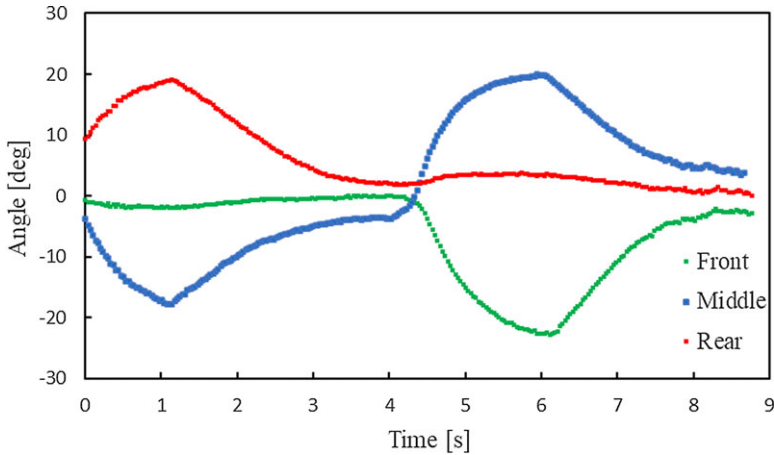
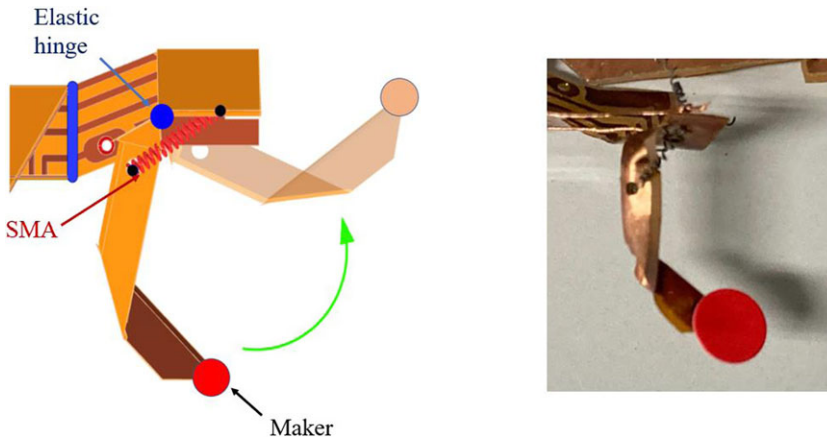**Figure 14.** *Operation angle and time for Mode 1.*

Figure 15. *Experimental setup for Mode 2 testing.*

The switching circuits of the foreleg or the hind leg were operated alternately with a load voltage of 1 V, a heating time of 2 s and a cooling time of 3 s. The movement angles of the legs were measured by image analysis using a camera. Fig. 13(b) shows the actual images taken during the experiment.

As shown in Fig. 14, the maximum driving angles were 22.8°, 19.9°, and 19.0° for the fore, middle, and hind legs, respectively. The driving distance was −1.64 mm for the front leg, −1.30 mm for the middle leg, and 1.38 mm for the rear leg, with the direction of travel as positive. The error in the values for each leg is considered a problem of assembly accuracy during folding and SMA attachment.

It was also confirmed that each leg can be restored to its initial position without any problem by the restoring force of the elastic hinge after the end of the movement, confirming that the Mode 1 motion, in which the legs move horizontally, can be driven by the contraction of the SMAs.

3.2.2. Driving experiment in operating Mode 2
In this experiment, a motion test was conducted on Mode 2, a vertical leg movement using SMA. As shown in Fig. 15, in Mode 2, the legs move up and down by the contraction of the SMA heated by electric current and the restoring force of the elastic hinge. Markers were attached to the toes of the legs, the motion was filmed using a camera, and the trajectory of the leg markers was measured by image analysis using Image-J. The trajectory of the markers was measured using the image analysis software.
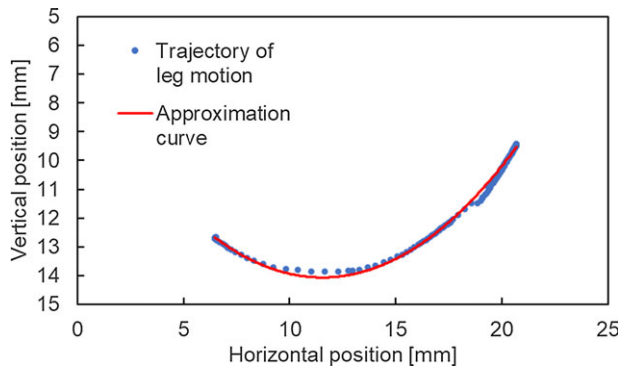
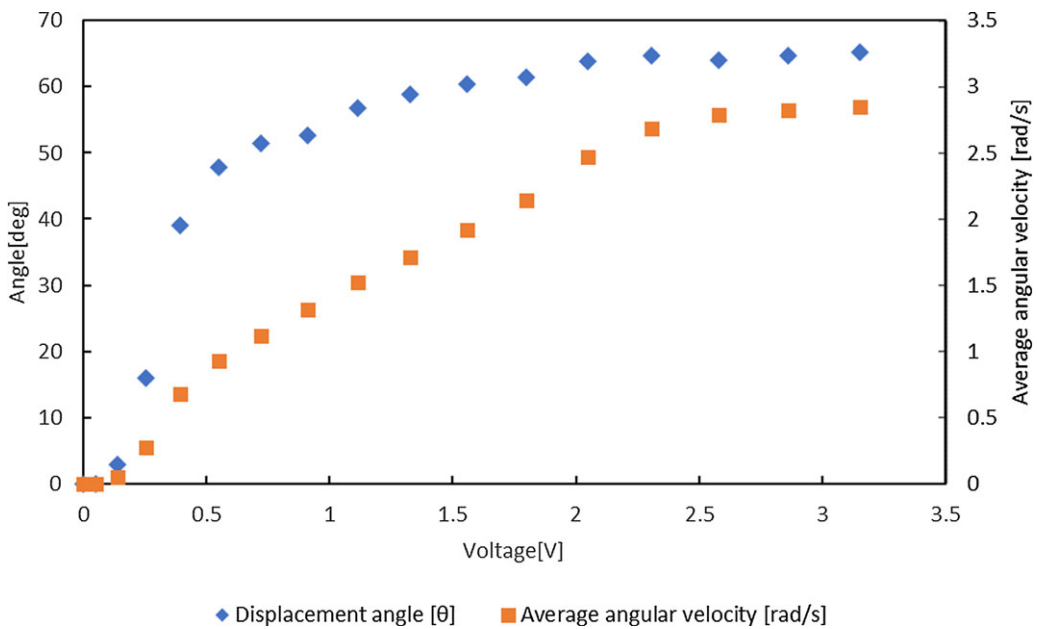**Figure 16.** *The toe movement trajectory.*

Figure 17. *Voltage and foot movement angle, movement speed.*

The measurement results confirmed that the maximum driving angle from the lowest point was 67° and the maximum movable distance of the toes was 4.5 mm in the vertical direction (Fig. 16). Additionally, the height of the lower part of the hexapod body from the ground was approximately 5.5 mm, and the toes could move approximately 82% of that height.

In the experiment on the voltage and operating angle using PWM control, the battery was used as a power supply voltage of 3.7 V, and the duty ratio was adjusted using PWM control to control the applied voltage. The amplitude is 3.7 V and the frequency is 490 Hz, sufficiently fast for the system response using SMA. The operation was confirmed using a Joule heating time of 1 s. Fig. 16 shows the applied effective voltage and operating angle of the toes. The operating angle increased sharply until the voltage on the horizontal axis reached approximately 0.6 V, then gradually increased and approached 65 DA;. The SMA (BMX100) used had a standard drive current of 100–150 mA and a standard electrical resistance of 900 Ω/m. The length of the SMA used in Mode 2 was about 5 mm, with a drive voltage of approximately 0.45 V–0.675 V. This was sufficiently driven by the operating circuit of the hexapod.

We also measured the applied effective voltage and average angular velocity of the toes (Fig. 17). The average angular velocity is calculated by dividing the operating angle between the initial position and the steady state when voltage is applied by the time it took to reach the steady state. The measurement results

confirmed that the speed increased gradually to 2.8 [rad/s] as the voltage increased. The figure also shows that the average angular velocity is proportional to the input Joule heat. From the above results, it is presumed that the operating angle and speed of the toes of the micro-hexapod can be controlled by controlling the applied voltage using PWM control.

4. Conclusions

In this study, we propose a micro-hexapod with an SU-8 rigid frame that can be assembled from a single sheet. By applying the SU-8 coating as a structure to the hexapod and increasing the rigidity, we succeeded in reducing the substrate size to within 40 mm square and the total length when assembled to approximately 30 mm. This enables the integration of the MEMS process into a small and inexpensive hexapod robot. In the MEMS process, Cu was patterned as a drive circuit and SU-8 was patterned as a structure to produce an SU-8 board. Hexapods can be assembled and manufactured by applying electrical equipment to an SU-8 board and folding it. In addition, driving experiments were conducted on Modes 1 and 2, which are walking motion modes, to realize a hexapod tripod walk. As a result of the experiment, it was confirmed that in Mode 1, the robot could move forward and backward, and could drive an average of 1.44 mm in one step; in Mode 2, it was confirmed that the robot could drive its toes up to 4.5 mm in the vertical direction, and a driving experiment on Mode 2, which is a leg raising motion, was conducted. As a result of the experiment, it was confirmed that the toes could be driven a maximum of 4.5 mm in the vertical direction. It is estimated that the operating angle and speed of the toe of the micro-hexapod can be controlled by the applied voltage using PWM control. Although there are currently some errors in each value depending on the accuracy of the assembly, it is estimated that walking motion is possible if the motion is controlled using PWM control in Mode 1 and Mode 2, which are the walking motion modes.

In this study, we successfully miniaturized and improved a hexapod that can be assembled from a single sheet and adapted to the MEMS process using SU-8 as the structure. In the future, we will apply the MEMS process to this hexapod further, aiming to improve the assembly accuracy and realize a tripod gait, which is a walking motion. We will also develop it as an inexpensive, mass-producible swarm search application tool with communication devices, sensors, and other devices.

References

[1] B. Goldberg, R. Zufferey, N. Doshi, E. F. Helbling, G. Whittredge, M. Kovac and R. J. Wood, "Power and control autonomy for high-speed locomotion with an insect-scale legged robot," *IEEE Robot. Autom. Let* **3**(2), 987–993 (2018).

[2] G.-P. Jung, C. S. Casarez, S.-P. Jung, R. S. Fearing and K.-J. Cho, "An Integrated Jumping-Crawling Robot using Height-Adjustable Jumping Module," **In:** *2016 IEEE International Conference on Robotics and Automation (ICRA)*, (2016) pp. 4680–4685.

[3] K. Sugita, M. Takato, K. Saito and F. Uchikoba, "Mechanical Structure for High Speed Locomotion of MEMS Microrobot Using SMA Rotary Actuator," **In:** *IECON. 2016 - 42nd Annual Conference of the IEEE Industrial Electronics Society*, (2016).

[4] M. Luneckas, T. Luneckas, J. Kriaučiūnas, D. Udris, D. Plonis, R. Damaševičius and R. Maskeliūnas, "Hexapod robot gait switching for energy consumption and cost of transport management using heuristic algorithms," *Appl. Sci* **11**(3), 1339 (2021).

[5] R. Sahai, S. Avadhanula, R. Groff, E. Steltz, R. J. Wood and R. S. Fearing, "Towards a 3g Crawling Robot Through the Integration of Microrobot Technologies," **In:** *Proceedings 2006 IEEE International Conference on Robotics and Automation*, (2006) pp. 296–302.

[6] C. Karakadıoglu, M. Askari and O. Ozcan, "Design and Operation of MinIAQ: An Untethered Foldable Miniature Quadruped with Individually Actuated Legs," **In:** *IEEE International Conference on Advanced Intelligent Mechatronics (AIM)*, (2017) pp. 247–252.

[7] Q. Sun, F. Gao and X. Chen, "Towards dynamic alternating tripod trotting of a pony-sized hexapod robot for disaster rescuing based on multi-modal impedance control," *Robotica* **36**(7), 1048–1076 (2018).

[8] J. Coelho, B. Dias, G. Lopes, F. Ribeiro and P. Flores, "Development and implementation of a new approach for posture control of a hexapod robot to walk in irregular terrains," *Robotica* **42**(3), 792–816 (2023).

[9] A. T. Baisch and R. J. Wood, "Robotics Research," **In:** *The 14th International Symposium (ISRR)*, (2011) pp. 715–730.

[10] A. T. Baisch, P. S. Sreetharan and R. J. Wood, "Biologically-Inspired Locomotion of a 2g Hexapod Robot," **In:** *2010 IEEE/RSJ International Conference on Intelligent Robots and Systems* (IEEE, 2010) pp. 5360–5365.

[11] Z.-Y. Wang, X.-L. Ding and A. Rovetta, "Analysis of typical locomotion of a symmetric hexapod robot," *Robotica* **28**(6), 893–907 (2010).

[12] T. Baisch and R. J. Wood, "HAMR3: Design and Fabrication of the Harvard Ambulatory Micro-Robot"," **In:** *Robotics Research the 14th International Symposium ISRR*, (2011) pp. 715–730.

[13] A. M. Hoover, E. Steltz and R. S. Fearing, "RoACH: An Autonomous 2.4 g Crawling Hexapod Robot," **In:** *2008 IEEE/RSJ International Conference on Intelligent Robots and Systems*, (2008) pp. 26–33.

[14] D. W. Haldane, K. C. Peterson, F. L. Garcia Bermudez and R. S. Fearing, "Animal-Inspired Design and Aerodynamic Stabilization of a Hexapedal Millirobot," **In:** *2013 IEEE International Conference on Robotics and Automation (ICRA)*, (2013) pp. 3279–3286.

[15] J. S. Lee and R. S. Fearing, "Anisotropic Collapsible Leg Spines for Increased Millirobot Traction," **In:** *2015 IEEE International Conference on Robotics and Automation (ICRA)*, (2015) pp. 4547–4553,

[16] D. W. Haldane and R. S. Fearing, "Running Beyond the Bio-Inspired Regime," **In:** *2015 IEEE International Conference on Robotics and Automation (ICRA)*, (2015) pp. 4539–4546.

[17] D. Yun and R. S. Fearing, "VLR: Cockroach millirobot with load decoupling structure," **In:** *2015 IEEE International Conference on Robotics and Automation*, (2015) pp.127–132.

[18] C. S. Casarez and R. S. Fearing, "Step Climbing Cooperation Primitives for Legged Robots with a Reversible Connection," **In:** *2016 IEEE International Conference on Robotics and Automation (ICRA)*, (2016) pp. 3791–3798.

[19] P. Birkmeyer, K. Peterson and R. S. Fearing, "DASH: A Dynamic 16g Hexapedal Robot," **In:** *2009 IEEE/RSJ International Conference on Intelligent Robots and Systems*, (2009) pp.2683–2689.

[20] D. Campbell and M. Buehler, "Stair Descent in the Simple Hexapod 'RHex'," **In:** *2003 IEEE International Conference on Robotics and Automation (ICRA)*, (2003) pp. 1380–1385.

[21] K. C. Galloway, G. C. Haynes, B. D. Ilhan, A. M. Johnson, R. Knopf, G. Lynch, B. Plotnick, M. White and D. E. Koditschek, X-RHex: A highly mobile hexapedal robot for sensorimotor tasks, (2010).

[22] S. Kim, J. E. Clark and M. R. Cutkosky, "ISprawl: Design and tuning for high-speed autonomous open-loop running," *Int. J. Robot. Res* **25**(9), 903–912 (2006).

[23] S. Kim, J. E. Clark and M. R. Cutkosky, "iSprawl: Autonomy, and the Effects of Power Transmission," **In:** *Climbing and Walking Robots*, (2005) pp. 859–867.

[24] R. J. Wood, "Design, Fabrication, and Analysis of a 3DOF, 3cm Flapping-Wing MAV," **In:** *2007 IEEE/RSJ International Conference on Intelligent Robots and Systems* (IEEE, 2007) pp. 1576–1581.

[25] M. Long, A. Gage, R. Murphy and K. Valavanis, "Application of the Distributed Field Robot Architecture to a Simulated Demining Task," **In:** *Proceedings of the 2005 IEEE International Conference on Robotics and Automation* (IEEE, 2005) pp. 3193–3200.

[26] K. Asamura and S. Nagasawa, "MEMS fabrication of compliant sheet for micro hexapod robots," *Japanese. J. Appl. Phys* **59**(SI), SIIL03 (2020).

[27] M. Askari, C. Karakadioglu, F. Ayhan and O. Ozcan, "MinIAQ-II: A Miniature Foldable Quadruped with an Improved Leg Mechanism," **In:** *2017 IEEE International Conference on Robotics and Biomimetics (ROBIO)*, (2017) pp. 19–25.

[28] C. Karakadıoğlu, M. Askari and O. Özcan. "Design and Operation of MinIAQ: An Untethered Foldable Miniature Quadruped with Individually Actuated Legs," **In:** *2017 IEEE International Conference on Advanced Intelligent Mechatronics (AIM)*, (2017) pp. 247–252.

[29] K. Asamura and S. Nagasawa, "A micro hexapod robot for swarm applications assembled from a single FPC sheet," *Japanese J. Appl. Phys.* **60**(SC), SCCL03 (2021).

[30] N. Lewis, A. York and S. Seelecke, "Experimental characterization of self-sensing SMA actuators under controlled convective cooling," *Smart Mater. Struc* **22**(9), 094012 (2013).

[31] A. Villoslada, A. Flores-Caballero, D. Copaci, D. Blanco and L. Moreno, "High-displacement fast-cooling flexible Shape Memory Alloy Actuator: Application to an Anthropomorphic Robotic Hand," **In:** *2014 IEEE-RAS International Conference on Humanoid Robots*, (2014) pp. 27–32.

[32] Shimoyama I., "Scaling in Microrobots," **In:** *Proceedings 1995 IEEE/RSJ International Conference on Intelligent Robots and Systems. Human Robot Interaction and Cooperative Robots*, (1995) pp. 208–211.

[33] C. D. Onal, M. T. Tolley, R. J. Wood and D. Rus, "Origami-inspired printed robots," *IEEE/ASME Trans Mechatro* **20**(5), 2214–2221 (2015).